Dynamic hybrid materials for constitutional self-instructed membranes

Adinela Cazacu, Yves-Marie Legrand, Andreea Pasc, Gihane Nasr, Arie Van der Lee, Eugene Mahon, and Mihail Barboiu[1]

Institut Européen des Membranes, Adaptive Supramolecular Nanosystems Group, Ecole Nationale Superieure de Chimie, Unité Mixte de Recherche 5635, Centre National de la Recherche Scientifique, University of Montpellier II, Place Eugène Bataillon, CC 047, F-34095 Montpellier, France

Edited by Virgil Percec, University of Pennsylvania, Philadelphia, PA, and accepted by the Editorial Board March 27, 2009 (received for review December 30, 2008)

Constitutional self-instructed membranes were developed and used for mimicking the adaptive structural functionality of natural ion-channel systems. These membranes are based on dynamic hybrid materials in which the functional self-organized macrocycles are reversibly connected with the inorganic silica through hydrophobic noncovalent interactions. Supramolecular columnar ion-channel architectures can be generated by reversible confinement within scaffolding hydrophobic silica mesopores. They can be structurally determined by using X-ray diffraction and morphologically tuned by alkali-salts templating. From the conceptual point of view, these membranes express a synergistic adaptive behavior: the simultaneous binding of the fittest cation and its anion would be a case of "homotropic allosteric interactions," because in time it increases the transport efficiency of the pore-contained superstructures by a selective evolving process toward the fittest ion channel. The hybrid membranes presented here represent dynamic constitutional systems evolving over time to form the fittest ion channels from a library of molecular and supramolecular components, or selecting the fittest ion pairs from a mixture of salts demonstrating flexible adaptation.

crown-ethers | ion channels | self-assembly

Many fundamental biological processes seem to depend on unique properties of hydrophilic domains of the membrane proteins (1, 2). Gramicidin A (3), KCsA-K^+ (4), and aquaporins (5) are well known nonexclusive examples of protein channels in which ions or water molecules diffuse along the directional pathways. Proteins that serve as ion channels contain simple inner functional moieties (i.e., carbonyl, hydroxyl, etc.), pointing toward the protein ion-transporting core, surrounded by the outer scaffolding protein wall orienting the transport direction. Artificial bilayer (6–10) or nanotube membrane systems (11–14) were developed during the last decades with the hope of mimicking the natural ion channels, to the direct benefit of the fields of chemical separations, sensors, or storage-delivery devices. Self-assembly is an elegant approach to constructing synthetic ion channels. It has already been shown that cations can template the formation of ion-channel columnar architectures. Seminal work by Percec *et al*. (15–20) has demonstrated the self-assembly of dendronized crown ethers into ion channels via complexation of cations. The G-quartet, the hydrogen-bonded macrocycle formed by the self-assembly of four guanosines, is stabilized by cations. Davis *et al*. (21–25) amply emphasized the role of cation templating in the stabilization of the G-quadruplex transporting device, the columnar architecture formed by the vertical stacking of four G-quartets. The same group showed that anion-directed self-assembly of calix[4]arenes generate chloride channels (26). Heteroditopic ureido crown ethers, reported by our group, self-organize in solution, in bilayer membranes, and in the solid state into columnar superstructures via complexation of both cations and anions (Fig. 1). Recently, we proved the possibility to create ion-conduction pathways by self-assembly (27–29), and the urea ribbons and a silica scaffolding matrix can be used to orient the directional transporting superstructures in hybrid membrane materials. Our previous studies on receptors covalently attached to the silica matrix focused on their potential ability to recognize ions or molecules (30–32) or to control the "fixed-site jumping" diffusion along the directional nanometric pathways (33–35). Expanding this work, we actually use silica mesopores as a scaffolding matrix to build such self-assembled ion-channel-type heteroditopic systems. In this context, herein, we present an oriented mesoporous silica membrane system in which macrocyclic self-organized architectures have been set up noncovalently (confined) within such scaffolding mesopores. Evidence that the membrane adapts and evolves its internal structure to improve its ion-transport properties is presented; the dynamic noncovalently bonded macrocyclic ion-channel-type architectures can be morphologically tuned by alkali-salt templating during the transport experiments or the conditioning steps. Because of their ability to undergo continuous change in constitution of their organic/supramolecular functional network in response to external ionic stimuli, these membranes express an adaptive behavior: the simultaneous binding of the fittest cation and its anion increase the transport efficiency of the pore-contained internal superstructures as they selectively evolve toward the "fittest" ion channel.

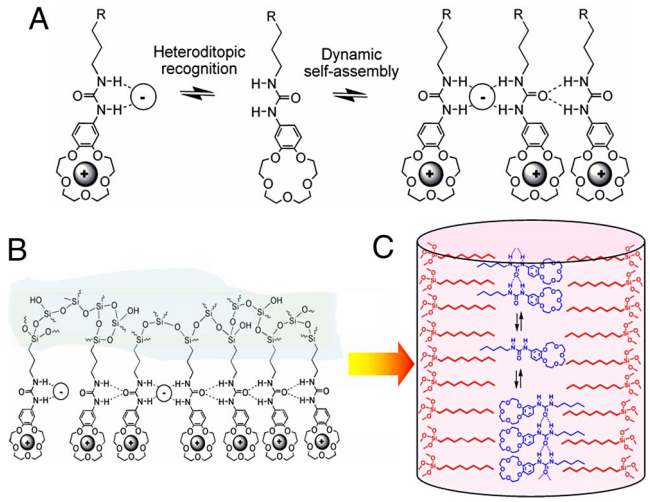

Fig. 1. From fixed-site to dynamic constitutional hybrid materials. (*A*) Dynamic self-organization and heteroditopic ion salts recognition of ureido-macrocyclic receptors. Generation of directional ion-conduction pathways: from fixed-site hybrid dense materials (*B*) to dynamic hybrid materials by the hydrophobic confinement within silica mesopores (*C*).

Author contributions: M.B. designed research; A.C. and E.M. performed research; A.C., Y.-M.L., A.P., G.N., and A.V.d.L. contributed new reagents/analytic tools; Y.-M.L., A.P., A.V.d.L., E.M., and M.B. analyzed data; and M.B. wrote the paper.

The authors declare no conflict of interest.

This article is a PNAS Direct Submission. V.P. is a guest editor invited by the Editorial Board.

Freely available online through the PNAS open access option.

[1]To whom correspondence should be addressed. E-mail: mihai.barboiu@iemm.univ-montp2.fr.

This article contains supporting information online at www.pnas.org/cgi/content/full/0813257106/DCSupplemental.

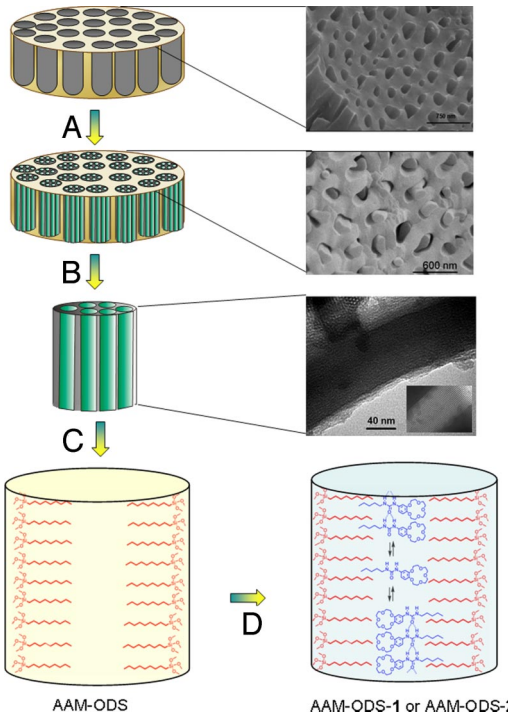

Fig. 2. Schematic representation of the synthetic route to obtain functionalized silica mesoporous AAMs filled with mesostructured silica-CTAB (arrow a), then calcinated (arrow b), reacted with hydrophobic ODS (arrow c), and finally filled with the hydrophobic carriers **1** or **2** (arrow d), resulting in the formation of MCM41-ODS-**1** and MCM41-ODS-**2** materials or of AAM-ODS-**1** and AAM-ODS-**2** membranes.

Results

Concept: Design of the Components. We recently focused attention on ureido benzo-crown ethers, leading by self-assembly in the absence or in the presence of ionic salts to columnar supramolecular architectures to enable efficient ion-translocation events in lipid bilayers (Fig. 1*A*) or in solid hybrid membranes (Fig. 1*B*) (27–29). Our efforts involve now the noncovalent binding of hexylureidobenzo-15-crown-5 (**1**) and hexylureidobenzo-18-crown-6 (**2**) macrocyclic receptors,confined in a lipophilic mesoporous silica scaffolding matrix (Fig. 1*C*), directionally oriented along the pores of the alumina Anodisc 47 (Whatman) membranes (AAMs) acting as supports (Fig. 2).

Synthesis of Mesoporous Dynamic Hybrid Materials and Membranes. In this work, the silica-filled AAMs were prepared with the template sol-gel method by using cetyltrimethylammonium bromide (CTAB) and tetraethohysilane as sol precursors to form silica mesopores oriented along the macropore walls of an AAM according to a previously reported procedure (Fig. 2, arrow a) (13). Afterward, a calcination step was performed to remove the CTAB (Fig. 2, arrow b). Such mesoporous silica-filled AAMs used for transport experiments as well as a reference mobile crystalline material 41 (MCM41)-type material (40-Å pore diameter) used for physical measurements were reacted with octadecyltrichlorosilane (ODS) (Fig. 2, arrow c) and then carefully washed to obtain the materials in which the hydrophobic ODS chains are covalently linked to the inner silica mesopore surface. Then, macrocyclic receptors **1** or **2** were noncovalently confined in the hydrophobic mesopores by immersing the hydrophobic materials and membranes in a chloroformic solution of **1**, **2**, or **1/2** (1/1, mol/mol), resulting in the formation of MCM41-ODS-**1** and MCM41-ODS-**2** materials and AAM-ODS-**1**, AAM-ODS-**2**, and AAM-ODS-{**1**, **2**} membranes (Fig. 2, arrow d, and Fig. S1).

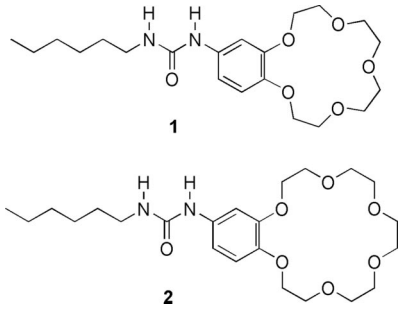

Scheme 1.

In Fig. 2, arrows a and b show that all AAM micropores are filled with silica mesoporous materials. The loss of scattering intensity in X-ray powder diffraction (XRPD) patterns and the decreasing of S_{BET} and V_{pores} values estimated from N_2 adsorption-desorption isotherms are strong evidence of the progressive covalent incorporation of ODS (a partial filling, 70%) and, furthermore, noncovalent confinement of the macrocyclic receptors **1** or **2** and **1/2** (1/1, mol/mol) (an almost complete filling, 98%) inside the silica mesopores (see *SI Appendix* and Figs. S2 and S3).

Confined Self-organization and Ion-Binding Behavior Within Mesopores. Further valuable insights on the confined organization of **1** and **2** and their ion-binding behaviors within the mesopores are obtained from the single-crystal structures and the XRPD of compounds **2**, **1**·KNO_3 (Fig. 3*A*), **2**·KNO_3 (Fig. 3*B*), and related MCM41-ODS-**1** and MCM41-ODS-**2** materials equilibrated with aqueous solutions of $NaNO_3$ and KNO_3. It is noted that silica materials are self-organized at a nanometric level, whereas the supramolecular organization is a result of specific columnar architectures of macrocyclic compounds. This hierarchical organization can be considered as a functional organization of the matter in which adaptive organic superstructures are oriented along a scaffolding silica inorganic matrix.

We have previously shown that in the solid state a dominant antiparallel packing of **2** via urea ribbons leads to extended stacks of crown ethers (27–29). Comparing the diffractograms generated from the single-crystal structure solution (Fig. 3*C*, red) with the experimental diffraction results of the bulk powder of **2** (Fig. 3*C*, blue), the preferential antiparallel packing (A) corresponding to the first (100) intense peak coexists in powder with a second residual parallel packing (P) corresponding to the second small peak, respectively. This residual peak is strongly amplified when **1** and **2** are confined in a hydrophobic MCM41-ODS material (Fig. 3*C*, dark cyan). We assume that the confinement of the macrocycles results in the formation of oligomers of parallel packing along the hydrophobic inner wall of the pore, whereas the antiparallel polymorphs are filling the central part of the pore.

To verify the compatibility of the bulk X-ray fingerprint with its single-crystal structures (Fig. 3*D*, red), bulk powders of **1**·KNO_3 (Fig. 3*E*, blue), **2**·KNO_3 (Fig. 3*D*, blue), MCM41-ODS-**1** (Fig. 3*D*, dark cyan), and MCM41-ODS-**2** (Fig. 3*E*, dark cyan) materials equilibrated with aqueous solutions of $NaNO_3$ or KNO_3 were investigated by XRPD. It is also important to notice that only when the crown ether-functionalized MCM41-ODS·**1** and MCM41-ODS·**2** materials were equilibrated with an aqueous solution of the fittest cation, NaCl or KCl, respectively, characteristic resolution and well defined diffraction peaks of complexes **1**·NaCl and **2**·KCl appeared, giving an indication as to its packing inside the material (see below the correlation with the single-crystal structures in Fig. 3 and Fig. S4). Additional peaks were found in all cases, and we suppose that polymorphic forms are present in the confined mesospace. It is also noted that the crystallinity is not extremely high in view of the broadness of the diffraction peaks. However, in all cases, a successful identification of the confined macrocyclic super-

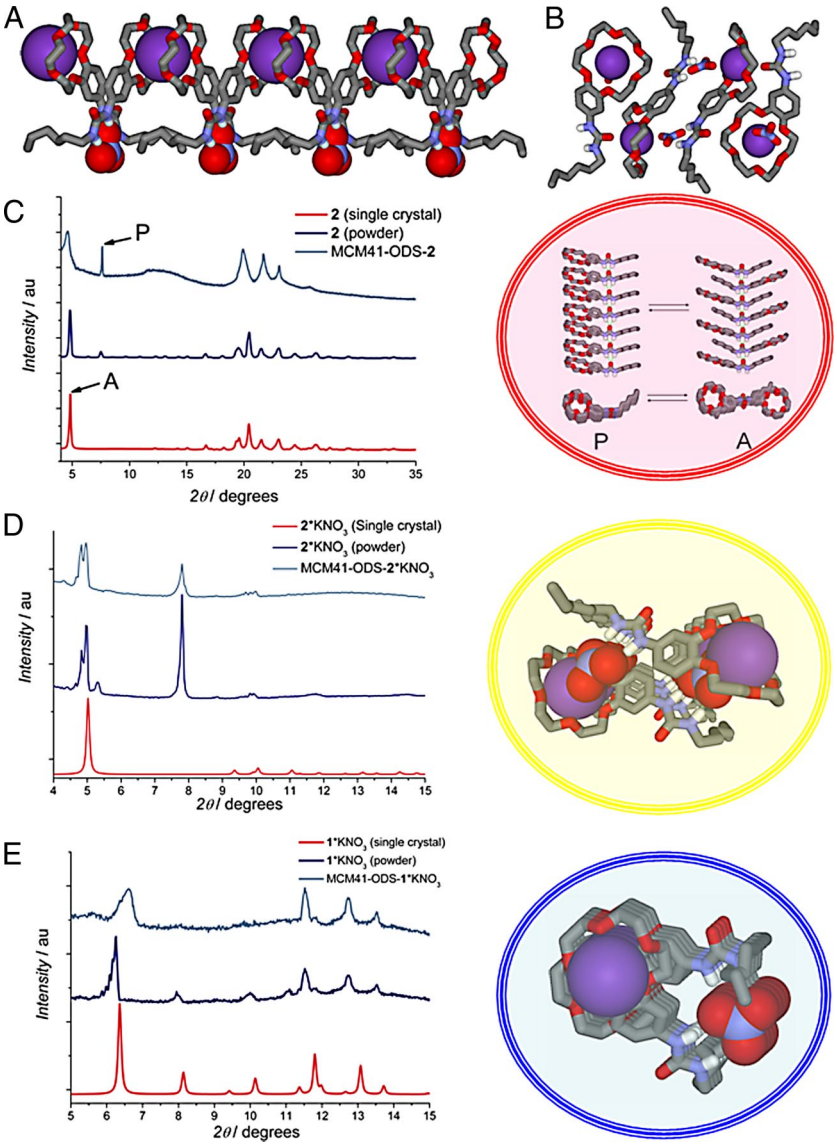

Fig. 3. Ion salt-binding behaviors within the mesopores. Shown are single-crystal structure and the crystal packing of **1**·KNO_3 (*A*) and **2**·KNO_3 (*B*) compounds: **1** and **2** in stick representation and K^+ and NO_3^- ions in Corey–Pauling–Koltun representation. Shown are single-crystal (red) and XRPD patterns of **2** (*C*, blue), **2**·KNO_3 (*D*, blue), **1**·KNO_3 (*E*, blue), AAM-ODS-**2**·KNO_3 (*D*, dark cyan), and AAM-ODS-**1**·KNO_3 (*E*, dark cyan) materials.

structures in the presence of ionic salts was achieved. The crystal structure of **2**·KNO_3 reveals that the heteroditopic antiparallel dimers (**2**·KNO_3)$_2$ are packed in close contact (Fig. 3 *B* and *D*). This structure alternates alignments of the host-cation-anion layers that are connected by apical coordinative bonds between the carbonyl moieties and K^+ cations. The difference between the calculated powder pattern of **2**·KNO_3 (red) with the experimental diffraction results of the bulk powder of **2**·KNO_3 (blue) and of the MCM41-ODS-**2**·KNO_3 material (dark cyan) (Fig. 3*D*) can be explained by either the presence of a second polymorphic phase or, most probably, a symmetry lowering of the crystalline phase in the bulk powder and in the hybrid material, assuming the formation of the nonconnected single layers aligned along the mesopore. Furthermore, it is noted that the same premise holds true for **1**·$NaNO_3$ (no single crystal available) and the MCM41-ODS-**1**·$NaNO_3$ material, which, from the XRPD data, have a similar structure to the **2**·KNO_3 and MCM41-ODS-**2**·KNO_3 systems.

In the crystal structure of **1**·KNO_3, the K^+ cations and the NO_3^- anions form the connecting bridges between macrocycles and reveal a "knotted" (**1**·KNO_3)$_n$ robust polymeric superstructure (Fig. 3*A*). It results in the formation of distinct solid-state ion channels for cations and anions, which are spatially separated in the crystal lattice as viewed down the central axes of the macrocycles (Fig. 3 *A* and *E*). Comparing the diffractogram generated from the single-crystal structure solution with the XRPD results, the bulk powders **1**·KNO_3 and MCM41-ODS-**1**·KNO_3 have similar structures to crystalline **1**·KNO_3.

These previously undescribed findings with respect to our previous work on the hybrid-dense materials (28, 32–35) is that the transporting nanostructures can accurately be determined by using single-crystal structures and XRPDs. These examples also show that this strategy can be used successfully to quantify and determine the overall self-organization of functional ion-channel-type superstructures confined within the hydrophobic mesoporous environment.

Membrane Transport Experiments. The primary goal of our work was to form oriented membrane ion-channel superstructures confined in a hydrophobic silica scaffolding nanospace taking advantage of the dynamic features of reversible connections between the formers' macrocyclic components. For this reason we have chosen to use heteroditopic receptors **1** and **2** with macrocyclic-cation and urea-anion binding sites, which can simultaneously bind ion pairs (27–29). The transport experiments, according to the solution-diffusion mechanism (Fick's law) were evaluated by using passive competitive conditions with both Na^+ and K^+ present in the feed phase and

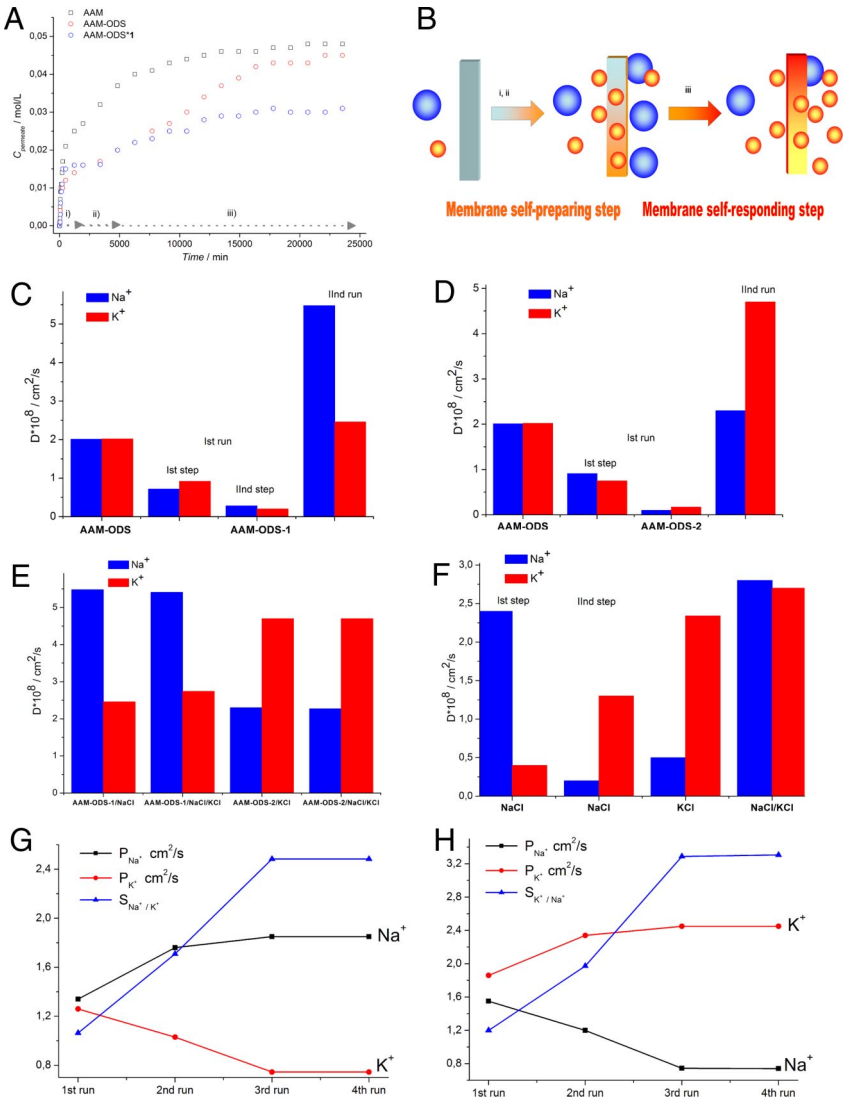

Fig. 4. Membrane transport experiments. (*A*) Concentration-versus-time plots of the permeating Na^+ ions transported through the AAM support and AAM-ODS-**1** membrane. (*B*) For the last experiment: (*i*) the first segment at short times represents the membrane self-preparing step in which the membrane retains the fittest cation (represented as orange spheres) and evolves its internal structure; (*ii*) mean transition step; and (*iii*) the last segment, at times longer than the transition step representing the membrane self-responding step, in which the transport of the fittest cation evolves to be more rapid and selective. Diffusion coefficients of competitive transport of Na^+ (blue) and K^+ (red) cations through AAM-ODS and functionalized AAM-ODS-**1** (*C*) and AAM-ODS-**2** (*D*) membranes; AAM-ODS-**1**·NaCl, AAM-ODS-**1**·NaCl/KCl, AAM-ODS-**2**·KCl, and AAM-ODS-**2**·NaCl/KCl conditioned membranes (*E*); and NaCl, KCl, NaCl/KCl AAM-ODS-{**1**, **2**} conditioned mixed membrane (*F*). Permeabilities and selectivities of the fittest cation Na^+ (*G*) and K^+ (*H*) are improved by performing repetitive transport experiments by using ion-conditioned AAM-ODS-**1**·NaCl and AAM-ODS-**2**·KCl membranes, respectively.

deionized water in the receiving phase, assuming that the chemical potential gradient across the membrane is only caused by a concentration gradient (30–35). The fitting of experimental receiving concentration versus time data allows the determination (see *SI Appendix*) of the permeability P_i, the diffusion coefficients D_i, and the partition coefficient ratio α_i of solute i.

In the absence of the macrocyclic receptors **1** and **2**, the Na^+ and K^+ salts are transported in a similar proportion through the AAM support and AAM-ODS membranes. In contrast, the hybrid AAM-ODS-**1** and AAM-ODS-**2** membranes show selective transport of salts (Fig. 4). Transport plots depicted in Fig. 4*A* show the concentration-versus-time profiles of the permeating Na^+ ions transported through the AAM support, hydrophobic AAM-ODS, and AAM-ODS-**1** membranes. When the AAM support is used for the transport we obtain the classical "initiation-diffusion-equilibrium" concentration-versus-time profiles for both Na^+ and K^+ cations (30–32).

The analogous transport plot for the AAM-ODS-**1** or AAM-ODS-**2** membranes containing macrocyclic-confined mesopores is slowed down and can be approximated as a sum of two classical profiles: (*i*) a first higher slope segment at short times followed by (*ii*) an equilibrium segment at mean transition times and then by (*iii*) a second lower slope segment at times longer than the transition step followed by the final equilibrium step (Fig. 4*A*). In the first step, the uptake of the cations is relatively fast ($\alpha > 1$); the overall transport is kinetically limited by the cation release from the membrane. The membranes are functioning like a sponge, presenting low diffusion coefficients (Table S1). In general, the transport of Na^+ and K^+ through the membrane is accompanied with the simultaneous complexation of the fittest cation (Na^+ for AAM-ODS-**1**, $D^+_{Na} < D^+_K$ and K^+ for AAM-ODS-**2**, $D^+_K < D^+_{Na}$, respectively) and of the anion, which are selectively retained into the membrane; it is the so-called membrane self-preparing step (Fig. 4 *A* and *B*).* Then, after the transition time, the transport only depends on the rate of diffusion of both cations ($\alpha = 1$). We observed that diffusion of the ion pairs corresponding to the fittest cation (Na^+ for AAM-ODS-**1**, $D^+_{Na} > D^+_K$ and K^+ for AAM-ODS-**2**, $D^+_K < D^+_{Na}$) occurs selectively much faster in the second stage: the so-called membrane self-responding step (Fig. 4*A* and *B*). The overall transport performances are clearly related to the first self-preparing step, during which the fittest cation is retained within the membrane while activating its transport for the second step. We

*The diffusion coefficients ($\approx 10^{-8}$) are of the same order of magnitude as those observed in dense membranes, and the time of observed effects during the transport experiments is strongly dependent on the thickness of the membrane (60 μm). The use of pressure-driven conditions or of thinner nanometric mesoporous films (see ref. 42) may reduce the diffusion time through the membranes presented here, which is beneficial for future applications.

have repeated the transport in a second run by using a fresh ionic solution (feed phase) and deionized water (receiving phase), and the mean transition step was no longer observed. After an induction time of ≈3000 min, in this second transport using the same membrane, the selectivity change in the favor of the salt of the fittest cation (Na^+ for AAM-ODS-**1** and K^+ for AAM-ODS-**2**) and the diffusion coefficients are strongly improved compared with those of the first run (Fig. 4 *C* and *D*, Table S1). The observed mean transition step and the selectivity change after the first run are reproducible, but they are very unusual for a classical diffusion transport experiment. The treatment of AAM-ODS-**1** and AAM-ODS-**2** membranes with the fittest cation salt seems to template the formation of specific ion-channel superstructures that happen to mediate (facilitate) the transport of the target cation/anion pairs through such preorganized channels under the driving force of chemical potential gradient. To illustrate this specific ion-channel formation, we have first of all conditioned the membranes with the fittest cation salt (NaCl for AAM-ODS-**1** and KCl for AAM-ODS-**2**) by submerging the membranes in an aqueous salt solution during 48 h. Then, in a second series of experiments, both membranes were conditioned in an equimolar solution of NaCl/KCl. All of these experiments show that the transport selectivity is in the favor of the salt of the fittest cation (Na^+ for AAM-ODS-**1** and K^+ for AAM-ODS-**2**) (Fig. 4*E*). The most surprising results concern the AAM-ODS-**1** membrane in which the hexylureidobenzo-15-crown-5 (**1**) receptor can complex both NaCl and KCl. We have shown before that structural organization of the pore-confined macrocyclic superstructures, in the absence or presence of the ionic salts, can be accurately determined by using X-ray techniques. The dimensional compatibility between crown-ether cavity and cation diameter is no longer effective in the case of such heteroditopic complexants; the receptor **1** forms a dimeric supramolecular polymer (Fig. 3, arrows b and d) in the presence of the salt of the fittest cation (AAM-ODS-**1**·Na^+) and a knotted oligomer (Fig. 3, arrows a and e) in the presence of the nonfittest cation (AAM-ODS-**1**·K^+). The simultaneous cation/anion co-complexation induces the formation of specific 3D ion channels for both the fittest (Na^+) and nonfittest (K^+) cations via macrocycles, together with the anion pathways via the urea moieties. The preferential "transporting superstructure" present in the AAM-ODS-**1** membrane environment during transport might correspond to the dimeric supramolecular polymer (Fig. 3*d*). In this superstructure, the fittest cation is bound equatorially by the macrocycle and the anion H-bonded to urea moiety, simultaneously occupying one cation's apical position so that the cation and the anion are spatially interacting together, to be transported as ion pairs, which might, in principle, favor the transport performances experimentally observed (Fig. 2, arrows b and d). In contrast, the nonfittest K^+ cation and the anion (Cl^-, NO_3^-) are sandwiched between two 15-crown-5 macrocycles and two urea groups, respectively. It results in the formation of a "knotted" oligomeric superstructure in which the cations and anions are not in contact. A potential drawback of that superstructure containing individual carrier-ion pathways is the Coulombic penalty that must be paid to enforce this charge separation (Fig. 2 arrows a and e). The transport experiments show that when merely saturated with both salts (NaCl/KCl), the fittest Na^+ cation signals the systems to produce more binding-favorable superstructure, even in the presence of the competitive K^+ cation (Fig. 4*E*). As expected, the hexylureidobenzo-18-crown-6 (**2**) receptor forms only the dimeric supramolecular polymer in the presence of the salt of the fittest K^+ cation (AAM-ODS-**2**·K^+). On the basis of these results, we would conclude that this system is closer to an "allosteric regulation" (36), wherein the simultaneous binding of the fittest cation and the anion effectors increases the transport efficiency of the pore-confined 3D superstructure generating the fittest ion channels in which ions are transported as ion pairs.

Then, the mixed membranes AAM-ODS-{**1**, **2**} filled with an equimolar mixture of **1** and **2** were separately conditioned with NaCl, KCl or NaCl/KCl, respectively, and the transport results are the following (Fig. 4*F*):

1. In the first step, the Na^+-conditioned mixed-membrane AAM-ODS-{**1**, **2**} selectively transports Na^+ over K^+ via the fittest AAM-ODS-**1**·NaCl channels, continually saturating the system with KCl. Then, in the second step, the diffusion of ions strongly decreases because of a lower difference of chemical potential gradient, but now the membrane transports selectively K^+ over Na^+ via the fittest AAM-ODS-**2**·KCl channels evolved during the first step.
2. The K^+-conditioned mixed-membrane AAM-ODS-{**1**, **2**} selectively transports K^+ over Na^+ via the fittest AAM-ODS-**2**·KCl channels, favored to inactive nontransporting AAM-ODS-**1**·KCl.
3. Moreover, the Na^+ and K^+ cations are transported in a similar proportion via active AAM-ODS-**1**·NaCl and AAM-ODS-**2**·KCl pore-confined channels when an AAM-ODS-{**1**, **2**} mixed membrane was conditioned with the NaCl/KCl mixture.

Finally, by repeating the transport experiments, although (AAM-ODS-**1**·Na^+) and (AAM-ODS-**2**·K^+) conditioned membranes, we found that in the next runs the permeabilities of the fittest cation were increasing while the permeabilities of the nonfittest cation were decreasing, presenting saturation behavior after the third experiment (Fig. 4 *G* and *H*). It results in a continuous increase in the selectivity (defined as the permeability ratio $P_{fittest}/P_{nonfittest}$) for the fittest cation, showing that the tradeoff in the low-permeability/high-selectivity, or vice versa, balance is not still present, as is generally observed for glassy polymers used for gas and ion separations.

Discussion

We describe in this article a dynamic membrane system in which a set of heteroditopic macrocyclic receptors generating ion-channel superstructures can organize in a directional inorganic scaffolding mesopore. The reversible interactions between functional macrocyclic compounds make them respond to external ionic stimuli and adaptive toward forming the most efficient transporting superstructure, in the presence of the fittest cation, selected from a set of diverse less-selective possible architectures formed in the presence of the nonfittest cation. In particular, the use of X-ray diffraction techniques to determine the pore-confined ion-channel superstructures is noteworthy and represents a useful strategy for correlating ion binding with transport activity based on structural insights. These 3D ion-channel superstructures happen to mediate transport via a hopping mechanism, as opposed to simple diffusion, which selectively enhances the transport of the fittest cation. Despite this specific diffusion, it is clear that the secondary cation is still being transported via a diffusion mechanism via empty space in the mesoporous substrate as evidence by little to no reduction in their transport rate.

The simultaneous binding of the fittest cation and its anion would be a case of "homotropic allosteric interaction" (36) as time as it increases the efficiency of the pore-confined superstructures selectively evolving (forming) to form the fittest ion channel. More generally, like in biology in which up-regulation means "the increase in the number of counts of a cellular component as response of external stimuli" (37), the chemical membrane systems described here undergo the spatial development (up-regulation) of the most adapted 3D ion-channel superstructure formed from molecular components' binding of the ion effectors (38, 39). Finally the results obtained extend the application of constitutional dynamic chemistry (40) from materials science to functional constitutional devices (41). The membrane AAM-ODS-**1** and mixed-membrane AAM-ODS-{**1**, **2**} systems represent dynamic constitutional systems evolving over time to form the fittest ion channels from a library of molecular and supramolecular components, or selecting the fittest ion pairs from a mixture of salts, demonstrating flexible adaptation. This feature offers to membrane science perspectives toward self-

designed materials evolving their own functional superstructure to improve their transport performances. Prospects for the future include the development of these original methodologies toward dynamic hybrid materials, presenting a greater degree of structural complexity. They might provide new insights into the basic features that control the design of new materials mimicking protein channels with applications in chemical separations or sensors or as storage-delivery devices.

Materials and Methods

Experimental Procedure and Full Characterization for Compounds 1 and 2. **1** and **2** were prepared as reported previously (29) by refluxing the hexyl isocyanate (**3**) and 4′-aminobenzo-15-crown-5 (**4**) or 4′-aminobenzo-18-crown-6 (**5**) (1.1/1 mol/mol) in CH3CN (5 h). After removal of the solvent, the residue was purified by flash chromatography (alumina/chloroform) and crystallized from *n*-hexane to afford **1** and **2** as white powders. The structural characterization data [NMR, electrospray ionization (ESI) MS, single-crystal X-ray structures] are in accord with proposed formulas (see *SI Appendix*).

Synthesis of Ionic Complexes of Macrocyclic Receptors 1 and 2 with MCl and MNO_3 Salts ($M^+ = Li^+$, Na^+, and K^+). The ligands **1** and **2** (20 mg) were dissolved in CD_3CN (2 ml), and excess of solid alkali salts were added to this solution, which was briefly sonicated and stirred overnight at 60°C. These solutions were monitored by ^1H NMR and ESI MS. Heteroditopic receptors **1** and **2** are able to extract solid Na*X* ($X = Cl^-$, NO_3^-) salts into CD_3CN as judged by changes in host NMR spectra consistent with the formation of exchanging receptor salt complexes. The largest downfield changes from 1.54 to 2.22 ppm ($NH_{aromatic}$) and from 1.24 to 1.70 ppm (NH_{alkyl}) are indicative of H-bonding of urea moiety with the anions. Evidence for the heteroditopic binding was gained by using ESI MS. For example, the mass spectra of **1**·NaCl showed peaks at *m/z* 426, 828, and 1231 corresponding to $[\mathbf{1}\cdot Na]^+$, $[\mathbf{1}_2\cdot Na]^+$, and $[\mathbf{1}_3\cdot Na_2]^+$ aggregates, respectively. Additional peaks corresponding to the higher stoichiometries including the anions: $[\mathbf{1}_n\cdot Na_{n-1}X_{n-2}]^+$, $n =$ 1–5 (positive ESI), and $[\mathbf{1}_n\cdot Na_{n+1}X_{n+1}\text{-}H]^-$ or $[\mathbf{1}_n\cdot Na_nX_{n+1}]^-$ $n = 1$–4 (negative ESI) were observed as well. Crystals suitable for X-ray structure determination of **1**·KNO_3 and **2**·KNO_3 were obtained after a few days in acetonitrile/*i*-propyl ether mixtures (see the single-crystal X-ray data in *SI Appendix*).

Synthesis of Mesoporous MCM41-Type Crown-Ether Functionalized Powders and Membranes. It was previously demonstrated that Whatman Anodisc alumina membranes (AAMs) can serve as an oriented support material to form silica-surfactant nanotubes with a perpendicular orientation of the mesopores to the surface of the support and consequently parallel to (along) the alumina pore walls (13). Therefore, we have applied this method for the preparation of the membranes described in this article. In the first step, the AAMs were filled in with surfactant (CTAB)-template silica sol and then calcinated to remove the CTAB. The resulting mesoporous silica-filled AAMs, as well as the commercially available reference MCM41-type material MESOSYL (Silicycle, Quebec City, Quebec, Canada), were reacted successively with octadecyltrichlorosilane-ODS to obtain the hydrophobic mesopores followed by the physical incorporation of hydrophobic carriers **1** or **2** within the mesopores (Fig. S3).

Dialysis Transport Procedure. Membrane transport experiments were performed with a bicompartmental device, magnetically stirred at room temperature (Fig. S5). It consists of a two-cell Teflon device separated by the solid membrane. Nitrogen-permeation measurements were performed to ensure that they were dense and defect free. The feed phase was an aqueous solution of a 10^{-1} M NaCl + 10^{-1} M KCl solution for the competitive cation-transport experiments. The membrane consisted of supported dense membrane ($S =$ 5.32 cm^2), whereas the receiving phase consisted of 50 ml of deionized water. The Na^+ and K^+ concentrations were monitored at different time intervals by using the atomic absorption spectrophotometry. The competitive transport of Na^+ and K^+ across the membranes according to the solution-diffusion mechanism was evaluated by using passive transport conditions (30–32).

ACKNOWLEDGMENTS. This work, conducted as part of the award ''Dynamic Adaptative Materials for Separation and Sensing Microsystems'' made under the European Heads of Research Councils and European Science Foundation EURYI (European Young Investigator Awards) scheme in 2004, was supported by funds from the Participating Organisations of EURYI and the European Commission Sixth Framework Programme (see www.esf.org/euryi).

1. Hucho F, Weise C (2001) Ligand-gated ion channels. *Angew Chem Int Ed* 40:3100–3116.
2. Vaitheeeswaran S, Yin H, Raisaiah JC, Hummer G (2004) Water clusters in nonpolar cavities. *Proc Natl Acad Sci USA* 101:17002–17005.
3. Cukierman S (2000) Proton mobilities in water and in different stereoisomers of covalently linked gramicidin A channels. *Biophys J* 78:1825–1834.
4. Mackinnon R (2004) Potassium channels and the atomic basis of selective ion conduction. *Angew Chem Int Ed* 43:4265–4277.
5. Agre P (2004) Water channels. *Angew Chem Int Ed* 43:4278–4290.
6. Gokel GW, Mukhopadhyay A (2001) Synthetic models of cation-conducting channels. *Chem Soc Rev* 30:274–286.
7. Voyer N (1996) The development of peptide nanostructures. *Top Curr Chem* 184:1–35.
8. Bong DT, Clark TD, Granja JR, Ghadiri MR (2001) Self-assembling organic nanotubes. *Angew Chem Int Ed* 40:988–1011.
9. Matile S (2001) En route to supramolecular functional plasticity: synthetic β-barrels, the barrel-stave motif, and related approaches. *Chem Soc Rev* 30:158–167.
10. Fyles TM (2007) Synthetic ion channels in bilayer membranes. *Chem Soc Rev* 36:335–347.
11. Kohli P, *et al.* (2004) DNA-functionalized nanotube membranes with single-base mismatch selectivity. *Science* 305:984–986.
12. Jirage KB, Hulteen J, Martin CR (1997) Nanotubule-based molecular-filtration membranes. *Science* 278:655–658.
13. Yamaguchi A, *et al.* (2004) Self-assembly of a silica–surfactant nanocomposite in a porous alumina membrane. *Nat Mater* 3:337–343.
14. Hinds BJ, *et al.* (2004) Aligned multiwalled carbon nanotube membranes. *Science* 303:62–65.
15. Percec V, *et al.* (1993) Molecular recognition directed self-assembly of supramolecular cylindrical channel-like architectures from 6,7,9,10,12,13,15,16-octahydro-1,4,7,10,13-pentaoxabenzocyclopentadecen-2-ylmethyl-3,4,5-tris(*p*-dodecyloxybenzyloxy)benzoate. *J Chem Soc Perkin Trans I* 13:1411–1420.
16. Percec V, Heck JA, Tomazos D, Ungar G (1993) The influence of the complexation of sodium and lithium triflate on the self-assembly of tubular architectures displaying a columnar mesophase based on taper-shaped monoesters of oligoethylene oxide with 3,4,5-tris[*p*-(*n*-dodecan-1-yloxy)bezyloxy]benzoic acid and of their polymethacrylates. *J Chem Soc Perkin Trans II* 12:2381–2388.
17. Percec V, *et al.* (1993) Self-assembly of taper-shaped monoesters of oligoethylene oxide with 3,4,5-tris[*p*-(*n*-dodecan-1-yloxy)bezyloxy]benzoic acid and of their polymethacrylates into tubular supramolecular architectures displaying a columnar mesophase. *J Chem Soc Perkin Trans I* 12:2799–2811.
18. Percec V, Kawasumi M (1993) Similarities and differences between the mesomorphic behaviour of oligomeric macrocyclics and of linear high relative molecular mass polyethers based on 1-(4′-hydroxybiphenyl-4-yl)-2-(4-hydroxy phenyl)butane and flexible spacers. *J Chem Soc Perkin Trans I* 12:1319–1344.
19. Johansson G, Percec V, Ungar G, Abramic D (1994) Molecular recognition directed self-assembly of tubular liquid crystalline and crystalline supramolecular architectures from taper shaped (15-crown-5) methyl 3,4,5-tris(*p*-dodecyloxy) benzoate. *J Chem Soc Perkin Trans I* 4:447–459.
20. Percec V, Johansson G, Ungar G, Zhou J (1996) Fluorophobic effect induces the self-assembly of semifluorinated tepered monodedrons containing crown-ethers into supramolecular columnar dendrimers which exhibit a hometropic hexagonal columnar liquid crystalline phase. *J Am Chem Soc* 118:9855–9866.
21. Davis JT, Spada GP (2007) Supramolecular architectures generated by self-assembly of guanosine derivatives. *Chem Soc Rev* 36:296–313.
22. Davis JT (2004) G-quartets 40 years later: from 5′-GMP to molecular biology and supramolecular chemistry. *Angew Chem Int Ed* 43:668–698.
23. Shi X, Fettiger JC, Davis JT (2001) Homochiral G-quadruplexes with Ba nut not with K: the cation programs enantiomeric self-recognition. *J Am Chem Soc* 123:6738–6739.
24. Kaucher MS, Harrell WA, Davis JT (2006) A unimolecular G-quadruplex that functions as a synthetic transmembrane Na^+ transporter. *J Am Chem Soc* 128:38–39.
25. Ma L, Melegari M, Collombini M, Davis JT (2008) Large and stable transmembrane pores from guanosine-bile acid conjugates. *J Am Chem Soc* 130:2938–2939.
26. Sidorov V, *et al.* (2002) Ion channel formation from a calyx[4]arene amide that binds HCl. *J Am Chem Soc* 124:2267–2278.
27. Barboiu M, Vaughan G, van der Lee A (2003) Self-organized heteroditopic macrocyclic superstructures. *Org Lett* 5:3073–3076.
28. Barboiu M, Cerneaux S, van der Lee A, Vaughan G (2004) Ion-driven ATP-pump by self-organized hybrid membrane materials. *J Am Chem Soc* 126:3545–3550.
29. Cazacu A, *et al.* (2006) Columnar self-assembled ureido crown ethers: an example of ion-channel organization in lipid bilayers. *J Am Chem Soc* 128:9541–9548.
30. Barboiu M, *et al.* (1999) A new alternative to amino acid transport: facilitated transport of L-phenylalanine by hybrid siloxane membrane containing a fixed site macrocyclic complexant. *J Membr Sci* 161:193–206.
31. Barboiu M, *et al.* (2000) Facilitated transport of organics of biological interest I: a new alternative for the amino acids separations by fixed-site crown-ether polysiloxane membranes. *J Membr Sci* 172:91–103.
32. Barboiu M, *et al.* (2000) Facilitated transport of organics of biological interest II: selective transport of organic acids by macrocyclic fixed site complexant membranes. *J Membr Sci* 174:277–286.
33. Arnal-Hérault C, Banu A, Barboiu M, Michau M, van der Lee A (2007) Amplification and transcription of the dynamic supramolecular chirality of G-quadruplex. *Angew Chem Int Ed* 46:4268–4272.
34. Arnal-Hérault C, *et al.* (2007) Functional G-quartet macroscopic membrane films. *Angew Chem Int Ed* 46:8409–8413.
35. Michau M, *et al.* (2008) Ion-conduction pathways in self-organized ureidoarene-heteropolysiloxane hybrid membranes. *Chem Eur J* 14:1776–1783.
36. Tsai C-J, del Sol A, Nussinov R (2009) Protein allostery, signal transmission and dynamics: a classification scheme of allosteric mechanisms. *Mol BioSyst* 5:207–216.
37. Ng K, Howells J, Pollard JD, Burke D (2008) Up-regulation of slow K^+ channels in peripheral motor axons: a transcriptional channelopathy in multiple sclerosis. *Brain* 131:3062–3071.
38. Giuseppone N, Lehn JM (2004) Constitutional dynamic self-sensing in zinc/polyiminofluorenes system. *J Am Chem Soc* 126:11448–11449.
39. Legrand YM, van der Lee A, Barboiu M (2007) Self-optimizing charge transfer energy phenomena in metallosupramolecular complexes by dynamic constitutional self-sorting, *Inorg Chem* 46:9540–9547.
40. Lehn JM (2007) From supramolecular chemistry towards constitutional dynamic chemistry and adaptative chemistry. *Chem Soc Rev* 36:151–160.
41. Barboiu M, Lehn JM (2002) Dynamic chemical devices: modulation of contraction/extension molecular motion by coupled ion binding/pH change induced structural switching. *Proc Natl Acad Sci USA* 99:5201–5206.
42. Walcarius A, Sibottier E, Etienne M, Ghanbaja J (2007) *Nat Mater* 6:602–608.